

# Random Field Ising Model In and Out of Equilibrium

Yang Liu and Karin A. Dahmen

*Department of Physics, University of Illinois at Urbana-Champaign, Urbana, IL 61801, USA*

(Dated: May 25, 2019)

We present numerical studies of zero-temperature Gaussian random-field Ising model (zt-GRFIM) in both equilibrium and non-equilibrium. We compare the no-passing rule, mean-field exponents and universal quantities in 3D (avalanche exponents, fractal dimensions and anisotropy measures) for the equilibrium and non-equilibrium transition. We show compelling evidence that these two transitions belong to the same universality class.

PACS numbers: 02.60.Pn, 75.10.Nr, 75.60.Ej, 64.60.Fr

As a prototypical model for magnets with quenched disorder, the random-field Ising Model (RFIM) has been intensively studied during the last thirty years [1]. Nevertheless, some theoretically and experimentally important questions are still not answered. For example, it is still controversial whether the non-equilibrium and equilibrium transitions of the zero-temperature RFIM belong to the same universality class. It has been found that within the error bars, some critical exponents of these two transitions seem to match in 3D [2, 3, 4] and even in 4D [4, 5, 6]. Also, the  $6 - \epsilon$  expansion for the critical exponents of the non-equilibrium transition maps to all orders in  $\epsilon$  onto that of the equilibrium case [7], though the  $6 - \epsilon$  expansion in equilibrium has been controversial for decades [8]. Recently, renormalization group type arguments were suggested to conjecture that the critical points in these two transitions correspond to the same fixed point in a more general parameter space [9, 10]. More interestingly, it has been shown that the ground state (GS) and the demagnetized state (DS) have the same exponents and scaling functions associated with the disorder dependent magnetization, i.e.  $M(R)$  curve [11]. We also notice that the critical exponents and scaling functions calculated from the demagnetization curve and the associated avalanche noise seem to match those obtained from the saturation loop, which suggests that the two non-equilibrium transitions belong to the same universality class [12].

In this paper, we report new results which indicate that the equilibrium (ground state) and non-equilibrium (saturation loop) transitions belong to the same universality class. This is rather unexpected since in non-equilibrium the system has history dependence while in equilibrium it doesn't, see Fig. 1. We also address some previous studies which came to the opposite conclusion.

The RFIM is defined by the Hamiltonian

$$\mathcal{H} = - \sum_{\langle i,j \rangle} J s_i s_j - \sum_i (H + h_i) s_i \quad (1)$$

where the spins  $s_i = \pm 1$  sit on a  $D$ -dimensional hypercubic lattice with periodic boundary conditions. To model disorders, quenched fields  $h_i$  are randomly chosen from a Gaussian distribution with mean zero and variance  $R$ .

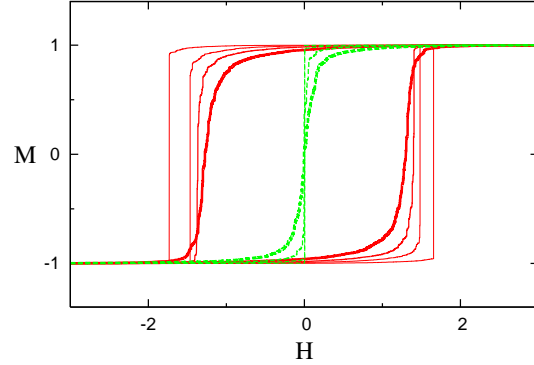


FIG. 1: Equilibrium (green-dashed) and non-equilibrium (red-solid) magnetization curves of the zt-GRFIM with system size  $32^3$  and various values of disorder: below, at and above  $R_c$ . ( $R_c^{eq} = 2.270 \pm 0.004$  [13] and  $R_c^{neq} = 2.16 \pm 0.03$  [4].) The thicker the line, the higher the disorder.

The temperature is set to zero and the external field  $H$  is increased adiabatically slowly from  $-\infty$  to  $\infty$ . Shown in Fig. 1 are the magnetization curves with different disorders. The non-equilibrium magnetization curves (hysteresis loops) are calculated using the local metastable dynamics, i.e. each spin flips deterministically when its effective local field  $h_i^{eff} = J \sum_j s_j + h_i + H$  changes sign. Three different algorithms to simulate this dynamics are described in Ref. 14. The equilibrium magnetization curves (GS evolutions) are obtained by using the efficient algorithm reported in Ref. 15, 16. This algorithm is essentially based on the fact that the GS energy has a convexity property which allows for estimates of the fields  $H$  where the magnetization jumps. To get the exact GS for a given disorder  $R$  at external field  $H$ , the RFIM GS problem is mapped onto the min-cut/max-flow problem in combinatorial optimization, which can be solved via the so-called push-relabel algorithm [17]. In both equilibrium and non-equilibrium, avalanches are associated with the magnetization jump during the magnetization process. Spin clusters are connected regions of flipped spins, formed by the aggregation of avalanches.

Before we show any numerical results about these two transitions, we show two extra similarities beyond critical

exponents obtained from 3D simulations. (1) *Middleton's no-passing rule* [18]: In non-equilibrium, this rule has been proved and applied to explain the return-point memory [19]. In equilibrium, the rule guarantees that no reverse spin flips occur in the magnetization curve when  $H$  is swept from  $-\infty$  to  $\infty$ . (Since flipped spins need not be considered any more in the GS calculation for all higher fields, the algorithm will be accelerated dramatically.) The proof follows. For any state  $C_2$  at field  $H_2$  which evolves from the GS  $C_1$  at field  $H_1$  ( $H_1 < H_2$ ) with reverse avalanches, we can always find a corresponding state  $\tilde{C}$  which evolves from  $C_1$  without any reverse avalanches and has lower energy than  $C_2$  at field  $H_2$ . So as  $H$  is increased, the GS evolves without any reverse spin flips (for details, see Ref. 20). (2) *Avalanche critical exponents in mean field theory*: It has been shown that in mean field theory (MFT) the two transitions have the same thermodynamic critical exponents ( $\beta$ ,  $\nu$ ,  $\delta$ ) [4, 21]. Here, we show that in MFT the avalanche critical exponents ( $\tau$  and  $\sigma$ ) should also be the same. We start the proof by noticing that in non-equilibrium the hard spin MFT magnetization curve has no hysteresis for  $R \geq R_c$ . Since there is only one  $M(H)$  solution for  $R \geq R_c$  in MFT, it is the non-equilibrium and the equilibrium solution at the same time. In MFT, every spin couples to  $M(H)$ . Since  $M(H)$  is unique, this implies that as  $H$  is increased there is a unique series of local-field configurations and therefore a unique series of states. This means that the avalanches in equilibrium must be the same for  $R \geq R_c$  as the avalanches in non-equilibrium. So the MFT avalanche exponents must be the same in both transitions.

Considering that these two transitions have the same no-passing property and the same MFT exponents (and exponent relations), one may think that the rough agreement of the two sets of thermodynamic critical exponents in 3D is just an accident. To shed some light on this issue, it is then necessary to check whether the critical behavior of these two transitions is different in some other aspects. This is the key motivation of this letter. We have studied system sizes ranging from  $L^3 = 32^3$  to  $192^3$  in all cases, except avalanches in equilibrium, where system sizes range from  $L^3 = 24^3$  to  $128^3$ . All the measured properties are averaged over a large number of realizations of the random-field configuration. Typical averages are performed over a number of realizations that ranges between  $10^4$  for  $L = 32$  and 50 for  $L = 192$ . Our main result is shown in Table I.

First, we extract the avalanche exponents from the field integrated avalanche size distribution  $D_{\text{int}}(S, R)$  associated with the equilibrium magnetization curve, see Fig. 2. The size  $S$  of an avalanche equals the number of spins participating in the avalanche. In both equilibrium and non-equilibrium, the scaling form of  $D_{\text{int}}(S, R)$

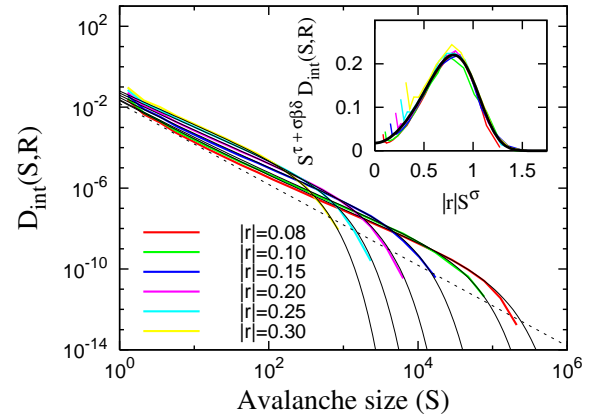


FIG. 2: Integrated equilibrium avalanche size distribution curves in 3D for  $64^3$  spins and different disorders. Those curves are averaged up to 500 initial random-field configurations. Here  $r = (R_c^{\text{eq}} - R)/R$  and  $R_c^{\text{eq}} = 2.27$ . The inset shows the scaling collapse of the integrated avalanche size distribution, using the equilibrium extrapolation values  $(\tau + \sigma\beta\delta)^{\text{eq}} = 2.00$  and  $\sigma^{\text{eq}} = 0.23$ . (With the non-equilibrium extrapolation values  $(\tau + \sigma\beta\delta)^{\text{neq}} = 2.03$  and  $\sigma^{\text{neq}} = 0.24$ , the scaling collapse still looks good.) The thick black curve through the collapse is the non-equilibrium universal scaling function  $\bar{D}_{\pm}^{\text{int}}(X)$  (see text). In the main panel, the equilibrium distribution curves obtained from the non-equilibrium scaling function are plotted (thin black lines) alongside the raw data (thick colored lines). The straight dashed line is the expected asymptotic power-law behavior:  $S^{-2.00}$ , which does not agree with the measured slope of the raw date due to the shape of the scaling function.

is given by

$$D_{\text{int}}(S, R) \sim S^{-(\tau + \sigma\beta\delta)} \bar{D}_{\pm}^{\text{int}}(S^{\sigma}|r|) \quad (2)$$

In non-equilibrium, this has been studied extensively, where  $(\tau + \sigma\beta\delta)^{\text{neq}} = 2.03 \pm 0.03$  and  $\sigma^{\text{neq}} = 0.24 \pm 0.02$  were obtained from scaling collapses and linear extrapolation to  $r = 0$  [4, 19]. In equilibrium, using the same method, we have  $(\tau + \sigma\beta\delta)^{\text{eq}} = 2.00 \pm 0.01$  and  $\sigma^{\text{eq}} = 0.23 \pm 0.01$ . We find that both  $\sigma^{\text{eq}}$  and  $(\tau + \sigma\beta\delta)^{\text{eq}}$  match to their non-equilibrium values within error bars. Furthermore, we find that the scaling functions match very well, see inset of Fig. 2. In Ref. 4, the non-equilibrium universal scaling function is obtained:

$$\begin{aligned} \bar{D}_{-}^{\text{int}}(X) = & e^{-0.789X^{1/\sigma}} (0.021 + 0.002X + \\ & + 0.531X^2 - 0.266X^3 + 0.261X^4) \end{aligned} \quad (3)$$

By plotting this non-equilibrium scaling function on top of the equilibrium scaling collapse, we find an excellent match, up to the overall horizontal and vertical scaling factor. According to this scaling function, we plot the distribution curves on top of the original data, we find excellent matches for all disorders. The match in both critical exponents and scaling functions strongly indicate that these two transitions belong to the same universality

TABLE I: Critical exponents and anisotropy measures obtained from numerical simulations in 3D for both equilibrium and non-equilibrium zt-GRFIM. Here, exponents in [ ] are quoted from Ref. 4. Exponents in ( ) are calculated with using  $l = l_{\text{gm}}$ .

Quantities	non-equilibrium		equilibrium	
	Avalanches	Clusters	Avalanches	Clusters
$\sigma$	[ $0.24 \pm 0.02$ ]		$0.23 \pm 0.01$	
$\tau + \sigma\beta\delta$	[ $2.03 \pm 0.03$ ]		$2.00 \pm 0.01$	
$d_S$	$2.81 \pm 0.02$ ( $2.76 \pm 0.03$ )	$2.77 \pm 0.03$ ( $2.75 \pm 0.03$ )	$2.85 \pm 0.01$ ( $2.71 \pm 0.03$ )	$2.81 \pm 0.02$ ( $2.76 \pm 0.03$ )
$d_v$	$2.81 \pm 0.02$ ( $2.76 \pm 0.03$ )	$2.77 \pm 0.03$ ( $2.75 \pm 0.03$ )	$2.85 \pm 0.01$ ( $2.72 \pm 0.03$ )	$2.81 \pm 0.02$ ( $2.76 \pm 0.03$ )
$d_a$	$2.35 \pm 0.02$ ( $2.32 \pm 0.03$ )	$2.20 \pm 0.02$ ( $2.18 \pm 0.03$ )	$2.20 \pm 0.01$ ( $2.13 \pm 0.02$ )	$2.13 \pm 0.01$ ( $2.10 \pm 0.02$ )
$A_1$	$0.286 \pm 0.010$		$0.300 \pm 0.020$	
$S_D$	$0.057 \pm 0.007$		$0.055 \pm 0.010$	
			$0.280 \pm 0.006$	
			$0.068 \pm 0.004$	

class. We note that in a previous work,  $(\tau + \sigma\beta\delta)^{\text{eq}} = 1.70 \pm 0.07$  was obtained via power-law fitting [22]. This shows that due to the “bump” in the scaling function, the power law exponent can not be extracted from a linear fit to the raw data since it will underestimate the exponent  $\tau + \sigma\beta\delta$ .

Second, we consider the spatial structure of both avalanches and clusters. In non-equilibrium, it has been found that near the critical point the spatial structure of avalanches is visually interesting [23]: (1) fractal (rugged on all scales); (2) anisotropic and topologically interesting. As for ground states, it has been found that near the critical disorder, spin clusters have fractal surfaces [13]. Here, we compute the fractal dimensions  $d_f$  of the size (or mass)  $S$ , enclosed volume  $v$  and outermost surface  $a$  of avalanches and clusters at  $R_c$  for both equilibrium and non-equilibrium. (Note that the difference between  $v$  and  $S$  is due to those possible “holes” inside avalanches or clusters [13].) Here, avalanches are integrated over the whole magnetization curve while clusters are chosen from states near the critical field  $H_c$ . For finite systems, the natural finite-size scaling hypothesis reads

$$f(l; R, L) = L^{d_f} \hat{f}(rL^{1/\nu}, l/L) \quad (4)$$

Here,  $f$  could be  $S$ ,  $v$  or  $a$  of the avalanche (or cluster) with linear size  $l$  in a system of linear size  $L$ .  $l$  can be defined as either the geometric mean ( $l_{\text{gm}}$ ) or the maximum ( $l_{\text{max}}$ ) of the lengths of the sides of the minimal rectilinear box that encloses the avalanche (or cluster) and has sides parallel to system sides.  $\nu$  is the critical exponent of the correlation length and  $\hat{f}$  is a universal scaling function. Eq. 4 enables us to do the scaling collapse at  $R_c$  for different system sizes. Extrapolation values ( $\langle L \rangle \rightarrow \infty$ ) are quoted in Table I. We find that  $d_S \cong d_v$  for all the cases, which indicates the “holes” would be ignorable in the large  $S$  (or  $v$ ) limit. We also notice that the extrapolation values with using  $l = l_{\text{gm}}$  and  $l = l_{\text{max}}$  are different. The difference gives us a sense of how big the systematic error could be. Considering this, we find that for both avalanches and clusters, their fractal dimensions ( $d_S$ ,  $d_v$  and  $d_a$ ) in equilibrium and non-equilibrium are very close. We can also use the discrete

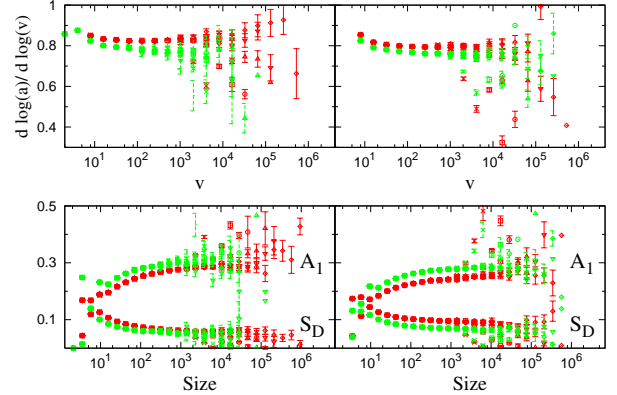


FIG. 3: (Top) Dependence of  $a$  of avalanches (left) and clusters (right) on  $v$  for both both equilibrium (green) and non-equilibrium (red) is expressed as an effective exponent  $(d \log a)/(d \log v)$ . (Bottom) Size dependent anisotropy measures of avalanches (left) and clusters (right) for both equilibrium (green) and non-equilibrium (red). Different symbols denotes different system sizes.

logarithmic derivative (DLD) to get the relative fractal dimension [13], e.g.  $d_a/d_v$ , see Fig. 3 (top). We plot  $(d \log a)/(d \log v)$  for different system sizes. The asymptotic values of the relative fractal dimensions are then obtained from the largest avalanches (or clusters) that are not affected by finite-size effects. We find that the asymptotic values for avalanches (or clusters) in equilibrium and non-equilibrium are very close.

For the anisotropy measures, as done in other systems, e.g. percolation and polymer chains, we use the radius of gyration tensor  $Q$  to characterize the shape of a given conformation of  $S$  points in  $D$ -dimensional space [24, 25, 26]:  $Q_{\alpha\beta} = \frac{1}{2S^2} \sum_{i,j=1}^S [X_{i,\alpha} - X_{j,\alpha}][X_{i,\beta} - X_{j,\beta}]$ . Here  $X_{i,\alpha}$  is the  $\alpha$ -coordinate of the  $i$ -th point with  $\alpha = 1, \dots, D$ . All the anisotropy measures are related to the  $D$  eigenvalues of the tensor  $Q$ :  $\lambda_\alpha$  with  $\bar{\lambda} = (\sum_\alpha \lambda_\alpha)/D$ . Here, we focus on two measures. A simple one:  $A_1 \equiv \lambda_D/\lambda_1$  and a complicated one: *prolateness*  $S_D \equiv (\lambda_1 - \bar{\lambda})(\lambda_2 - \bar{\lambda})(\lambda_3 - \bar{\lambda})/(2\bar{\lambda}^3)$ .  $S_D$  can be used to distinguish prolate (positive  $S_D$ ) from oblate shapes (negative  $S_D$ ) in  $D = 3$ . Results are shown in Fig. 3.

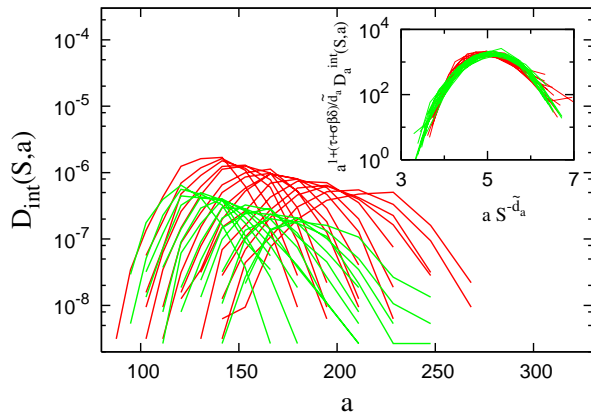


FIG. 4: Avalanche surface area distribution curves in 3D for  $192^3$  spins in non-equilibrium (red lines, averaged over 45 initial random-field configurations) and  $64^3$  spins in equilibrium (green lines, averaged over 1431 initial random-field configurations) for size  $S$  ranges from 50 to 88. The inset shows the scaling collapse of curves in the main panel, using the same set of exponents for both equilibrium and non-equilibrium:  $\tilde{d}_a = 0.81$ ,  $\tau + \sigma\beta\delta = 2.01$ .

It is interesting to mention that avalanches and clusters are prolate for both equilibrium and non-equilibrium. Asymptotic values of those anisotropy measures in the large size limit can be obtained similarly as we did for the relative fractal dimensions. We find that for both avalanches and clusters, the asymptotic values in equilibrium and non-equilibrium are very close, see Table I.

At last, we measure the distribution of surface areas integrated over the field  $H$  for each avalanche size  $S$  in both equilibrium and non-equilibrium. Analogous to the avalanche time distribution [4], the scaling form of surface area distribution can be written as:

$$D_a^{(int)}(S, a) \sim a^{-(\tau + \sigma\beta\delta + \tilde{d}_a)/\tilde{d}_a} D_a^{(int)}(a/S^{\tilde{d}_a}) \quad (5)$$

with  $\tilde{d}_a \equiv d_a/d_S$ . Fig. 4 shows the surface area distributions for different avalanche sizes and collapses of those curves using Eq. 5. With the same set of exponents for both equilibrium and non-equilibrium:  $\tilde{d}_a = 0.81$ ,  $\tau + \sigma\beta\delta = 2.01$ , the scaling functions match well, see inset of Fig. 4.

In sum, we have shown that the equilibrium and non-equilibrium transition of the zt-GRFIM behave similarly in three aspects. (1) The integrated size distribution of the avalanches: both the exponents and scaling functions match. (2) The spatial structure of avalanches and clusters: both fractal dimensions and anisotropy measures are very close in the large size limit. (3) The integrated surface area distribution of avalanches: same set of exponents for equilibrium and non-equilibrium yields quite similar scaling functions. All these results indicate that those two transitions are very likely in the same universality class. Larger system sizes could be a direct way to test it, especially for the fractal dimensions and anisotropy

measures. Analytic studies would be necessary to finally resolve this problem.

We thank James P. Sethna, Andrew Dolgert, A. Alan Middleton, Y. Oono, J. Carpenter, R. White, M. Delgado, and G. Poore for valuable discussions. We acknowledge the support of NSF Grant No. DMR 03-14279 and NSF Grant No. DMR 03-25939 ITR (Materials Computation Center). This work was conducted on the Beowulf cluster of the Materials Computation Center at UIUC.

---

- [1] A. P. Young, ed., *Spin Glasses and Random Fields*, vol. 12 of *Series on Directions in Condensed Matter Physics* (World Scientific, 1998).
- [2] A. Maritan, M. Cieplak, M. R. Swift, and J. R. Banavar, Phys. Rev. Lett. **72**, 946 (1994).
- [3] J. P. Sethna, K. Dahmen, S. Kartha, J. A. Krumhansl, O. Perković, B. W. Roberts, and J. D. Shore, Phys. Rev. Lett. **72**, 947 (1994).
- [4] O. Perković, K. A. Dahmen, and J. P. Sethna, Phys. Rev. B **59**, 6106 (1999).
- [5] A. K. Hartmann, Phys. Rev. B **65**, 174427 (2002).
- [6] A. A. Middleton, cond-mat/0208182 (2002).
- [7] K. Dahmen and J. P. Sethna, Phys. Rev. B **53**, 14872 (1996).
- [8] D. E. Feldman, Phys. Rev. Lett. **88**, 177202 (2002).
- [9] F. J. Pérez-Reche and E. Vives, Phys. Rev. B **70**, 214422 (2004).
- [10] E. Vives, M. L. Rosinberg, and G. Tarjus, Phys. Rev. B **71**, 134424 (2005).
- [11] F. Colaiori, M. J. Alava, G. Durin, A. Magni, and S. Zapperi, Phys. Rev. Lett. **92**, 257203 (2004).
- [12] J. H. Carpenter and K. A. Dahmen, Phys. Rev. B **67**, 020412 (2003).
- [13] A. A. Middleton and D. S. Fisher, Phys. Rev. B **65**, 134411 (2002).
- [14] M. C. Kuntz, O. Perković, K. A. Dahmen, B. W. Roberts, and J. P. Sethna, Comp. Sci. Eng. **1**, 73 (1999).
- [15] A. K. Hartmann, PHYSICA A **248**, 1 (1998).
- [16] C. Frontera, J. Goicoechea, J. Ortín, and E. Vives, J. Comp. Phys. **160**, 117 (2000).
- [17] B. Cherkassky and A. V. Goldberg, Algorithmica **19**, 390 (1997).
- [18] A. A. Middleton, Phys. Rev. Lett. **68**, 670 (1992).
- [19] J. P. Sethna, K. Dahmen, S. Kartha, J. A. Krumhansl, B. W. Roberts, and J. D. Shore, Phys. Rev. Lett. **70**, 3347 (1993).
- [20] Y. Liu and K. A. Dahmen, to be published (2006).
- [21] T. Schneider and E. Pytte, Phys. Rev. B **15**, 1519 (1977).
- [22] C. Frontera and E. Vives, Comp. Phys. Comm. **147**, 455 (2002).
- [23] J. P. Sethna, K. A. Dahmen, and C. R. Myers, Nature **410**, 242 (2001).
- [24] F. Family, T. Vicsek, and P. Meakin, Phys. Rev. Lett. **55**, 641 (1985).
- [25] J. A. Aronovitz and M. J. Stephen, J. Phys. A: Math. Gen. **20**, 2539 (1987).
- [26] E. E. O. Jagodzinski and K. Kremer, J. Phys. I France **2**, 2243 (1992).